THE JOURNAL OF PHYSICAL CHEMISTRY A

Article

pubs.acs.org/JPCA

Effects of Structural Differences on the NMR Chemical Shifts in Isostructural Dipeptides

Benjamin D. Altheimer and Manish A. Mehta*

Department of Chemistry and Biochemistry, Oberlin College, 119 Woodland Street, Oberlin, Ohio 44074, United States

Supporting Information

ABSTRACT: Porous crystalline dipeptides have gained recent attention for their potential as gas-storage materials. Within this large class is a group of dipeptides containing alanine, valine, and isoleucine with very similar crystal structures. We report the ^{13}C (carbonyl and Cα) and ^{15}N (amine and amide) solid-state NMR isotropic chemical shifts in a series of seven such isostructural porous dipeptides as well as shift tensor data for the carbonyl and amide sites. Using their known crystal structures and aided by ab initio quantum chemical calculations for the resonance assignments, we elucidate trends relating local structure, hydrogen-bonding patterns, and chemical shift. We find good correlation between the backbone dihedral angles and the Cα1 and Cα2 shifts. For the C1 shift tensor, the δ_{11} value shifts downfield as the hydrogen-bond distance increases, δ_{22} shifts upfield, and δ_{33} shows little variation. The C2 shift tensor shows no appreciable correlation with structural parameters. For the N2 tensor, δ_{11} shows little dependence on the hydrogen-bond length, whereas δ_{22} and δ_{33} both show a decrease in shielding as the hydrogen bond shortens. Our analysis teases apart some, but not all, structural contributors to the observed differences the solid-state NMR chemical shifts.

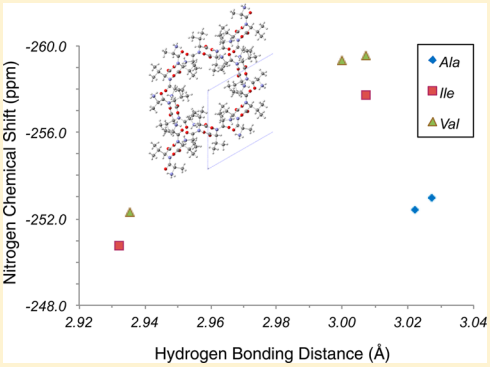

INTRODUCTION

The relationship between the structure of a molecular solid in the crystalline state and the chemical shift of its NMR-active nuclei has been of much interest to the NMR community. The isotropic chemical shift as well as the chemical shift anisotropy of the reporter nucleus can reveal a wealth of information, as they are sensitive probes of the local electronic environment. For proteins in solution, chemical shifts have been used in determining global 3D structure. This is done, for example, by predicting secondary structure,[1] by comparison to the chemical shifts of known structure,[2] and by using chemical shift data to constrain certain geometrical parameters[3−6] or as additional constraints during refinement when coupled with chemical shift calculations.[7] This approach has been made possible by a systematic compilation of chemical shifts in proteins,[8−12] detailed investigations of amino acids and peptides as model systems,[6,13−17] and various computational studies.[5,18−20] The connection between chemical shift and local structure for proteins in solution is sufficiently advanced that, in favorable cases, full structures can now be determined using chemical shifts alone.[1] Such a connection, however, is far less developed for peptides and proteins in the solid state because of the loss of spatial isotropy as well as the intermolecular interactions that stem from hydrogen bonding and noncovalent packing forces.

Understanding trends in chemical shifts is vital to the growing field of NMR crystallography in which a synergistic combination of diffraction and NMR data is used to investigate crystalline materials.[21] This approach is helpful for structures that cannot be solved by diffraction alone, which is often the case when only polycrystalline powders or no crystals are available. By combining chemical shifts with the known molecular identity of a crystalline compound, it is possible to constrain molecular geometries, to build initial models, and to evaluate the quality of models under subsequent refinement.[21] For example, chemical shifts have been used to predict backbone angles of amyloid fibrils and to build structure models of benzoxazine oligomers.[22,23] Hydrogen-bond lengths have also been determined using experimental and calculated chemical shifts,[24] and relative hydrogen-bonding strengths in multiple polymorphs of an amino acid derivative have been determined using chemical shift trends.[25] Further developing our understanding of these trends could eliminate or reduce the need for computational work.

Although many previous researchers have studied relationships between structure and chemical shift in the solid state, few have compared chemical shift data across similar structures. Even small changes in the chemical structure can lead to large rearrangements of the crystal structure to accommodate additional atoms. Thus, chemically similar molecules do not, in general, have similar crystal structures. In this work, we study a series of seven dipeptides, with known crystal structures, to further our understanding of how changes in structure affect ^{13}C and ^{15}N solid-state NMR chemical shifts. Peptides in this group all belong to the same crystallographic space group and

Received: November 14, 2013
Revised: March 18, 2014
Published: March 21, 2014

   dx.doi.org/10.1021/jp411220y | J. Phys. Chem. A 2014, 118, 2618−2628

have very similar unit cell dimensions; thus, we call this an isostructural series. They are part of a larger class of porous dipeptides identified by Görbitz,[26] which have been the focus of intense scrutiny as possible gas-storage materials.[27,28] The side chains of alanine, valine, and isoleucine containing dipeptides in our isostructural series form the walls of 1D pores,[29] which can accommodate side chains of various sizes. The variations in this set of seven dipeptides provide an opportunity to study chemical shift trends experimentally while keeping most structural parameters nearly constant. We report the isotropic ^{13}C and ^{15}N chemical shifts and the chemical shift tensors of carbonyl carbon atoms and nitrogen atoms of all seven of these dipeptides. We then consider correlations between chemical shift, peptide conformations, and hydrogen-bonding geometries.

EXPERIMENTAL SECTION

Sample Preparation. The seven dipeptides, L-valine-L-alanine (Val-Ala), L-alanine-L-valine (Ala-Val), L-alanine-L-isoleucine (Ala-Ile), L-isoleucine-L-alanine (Ile-Ala), L-valine-L-valine (Val-Val), L-valine-L-isoleucine (Val-Ile), and L-isoleucine-L-valine (Ile-Val), were obtained from Bachem. Following recrystallization from water, samples were hand ground in a mortar and pestle to produce polycrystalline powders. For Ala-Val and Val-Ala, previous work has not found water in the pores immediately following recrystallization from water.[27] The other samples were dried for at least 12 h under vacuum to remove any residual water from the pores.[30]

Powder X-ray diffraction (PXRD) was then used to verify the crystalline polymorph. PXRD patterns were collected using a Rigaku Ultima IV powder diffractometer (Cu Kα, 1.504 Å) with aluminum sample holders. Patterns were collected from 5 to 60° 2θ with a scan rate of 4° min^{-1} and a 0.02° sampling window. CrystalMaker and CrystalDiffract were used to calculate expected powder patterns from the crystal structures. These were compared to the experimental patterns to verify the polymorph.

Dry samples, approximately 70−90 mg, were packed in 4 mm silicon nitride rotors. Following packing, for all peptides except Ala-Val, the sample was again placed under vacuum for at least 3 h before closing the rotor end-cap under ambient conditions. Placing the Ala-Val rotor under vacuum later resulted in no change in the NMR spectrum.

Crystal Structures. The crystal structures of all seven dipeptides were obtained from the Cambridge Structural Database (CSD).[31] For better comparison to the room-temperature solid-state NMR data, room-temperature crystal structures were used. The CSD reference codes for each of these structures are given in Table 1. Single-crystal X-ray diffraction data was collected at room temperature on an Ala-Val crystal by Dr. Matthias Zeller at Youngstown State University. The resulting new structure of Ala-Val was used in this work. It is consistent with the published structure but treats the disorder in a manner more appropriate for the chemical shift calculations. The crystal structures were analyzed, and the torsion angles and hydrogen-bonding distances were measured using CrystalMaker.

NMR Measurements. The solid-state NMR experiments were performed on a custom-assembled NMR spectrometer with a Discovery console (Tecmag; Houston, TX), 14.1 T magnet (600.381 MHz for ^{1}H; Magnex Scientific; Oxford, England), a 39-channel matrix shim system (Resonance Research, Inc.; Billerica, MA), and a triple-resonance 4 mm magic angle spinning (MAS) probe (Doty Scientific Inc.; Columbia, SC). The MAS speed was regulated to ±2.5 Hz using a custom-built controller.

Cross-polarization magic angle spinning (CP/MAS) carbon spectra were collected for all samples at 3, 4, and 5 kHz. The ^{15}N spectra were collected at 1 and 8 kHz. Additionally, ^{15}N spectra of Val-Ala were collected at 0.8 and 1.2 kHz in order to estimate uncertainties in the principal values of the chemical shift anisotropy (CSA) tensor. A standard pulse sequence consisting of a 90° pulse on the proton channel, cross-polarization from proton to carbon or nitrogen, and then detection of the free-induction decay (FID) with proton decoupling was used. Typical CP parameters include a 20% power ramp in the carbon or nitrogen power level and a 2 ms contact times. Proton power levels during the CP were optimized for each sample and spin speed. High-power broadband decoupling (~100 kHz, SPINAL-64)[32] was applied on the proton channel. Because the drift rate of the magnet is very low (<0.1 Hz/day for ^{1}H), no counter ramp was required for the Z_0 shims. A 5 s recycle delay was used between scans. For most spectra, 4096 scans were collected to obtain an excellent signal-to-noise ratio and to improve the quality of the determined chemical shift tensor principal values. For the 1 kHz ^{15}N spectra, 32 768 scans were collected.

All spectra were processed using the software NTNMR. Baseline correction, two zero fills, and 5 Hz exponential apodization were applied. Zero-order and first-order phase corrections were applied as needed. Carbon spectra were externally referenced to 0.5% DSS (4,4-dimethyl-4-silapentane-1-sulfonic acid) in D_2O under MAS using the downfield resonance of solid adamantane under MAS at 40.490 ppm as a secondary standard.[33] Nitrogen spectra were externally referenced to neat nitromethane under MAS using the resonance of solid $^{15}NH_4Cl$ under MAS at −341.168 ppm.[34]

The CSA principal values were determined using the intensities of the spinning side bands via the Herzfeld−Berger method.[35] Side-band intensities were found by numerically integrating the isotropic and side-band resonances using a custom-written MatLab script. The integrated areas were used to fit the chemical shift tensor principal values using the software HBA.[36] To estimate the uncertainty associated with each value, the carbon CSA values were determined using three spin rates for all samples. The uncertainties quoted in this work for the carbon CSA values are the standard deviation of the mean (SEM) for these three measurements. Nitrogen spectra were collected at three spin speeds for Val-Ala to estimate the uncertainty. The uncertainties quoted for all nitrogen CSA values are the standard deviation in these three measurements.

NMR Calculations. Chemical shifts were calculated using the software CASTEP[37] and NMR-CASTEP[38,39] in Materials Studio 5.5. The CSD structures listed in Table S2 were used as a starting point for all calculations except for that of Ala-Val, for which the newly determined structure was used. The hydrogen atom positions were relaxed using constrained geometry optimization. For this calculation, the plane wave cutoff energy was 260 eV, 1 *k*-point was used, and the optimization was continued until energy changes below 5×10^{-6} eV cell^{-1} and displacements below 0.001 Å were observed. Chemical shieldings were calculated using a plane wave energy cutoff of 650 eV, 1 *k*-point, and on-the-fly pseudopotentials. Increasing the quality of the calculation by increasing the cutoff energy or number of *k*-points did not significantly change the resulting shieldings for Ala-Val. Because the required parameters for

Table 1. Backbone and First Side-Chain Torsion Angles of the Dipeptides along with Their CSD Codes[a]

Dipeptide	ψ_1 (°)	ω (°)	φ_2 (°)	ψ_T (°)	χ_{11} (°)	CSD reference code	ref
Ala-Val	158.0	178.4	−132.8	−35.7		XUDVOH01[b]	27
Val-Ala	165.0	175.1	−147.4	−30.7	54.7	WIRYEB02	27
Ala-Ile	154.5	176.8	−128.6	−41.7		HEGLOV	30
Ile-Ala	163.6	176.1	−152.8	−30.2	51.6	AQARUF01	30
Val-Ile	165.0	−179.2	−138.4	−24.9	57.9; −72.5	HEGMEM	30
Ile-Val	170.4	178.4	−139.3	−25.2	56.4	HEGMAI	30
Val-Val	165.2	−179.0	−138.8	−26.3	56.3	HEGLUB	30

[a]For consistency, ψ_T was always measured using O2. For the disordered side-chain values, angles are given in order of decreasing occupancy. [b]For Ala-Val, a newly determined structure was used. Note that weighted averages are used for the backbone angles for Ala-Val as the structure is disordered for some of the backbone atoms. The values for each configuration can be found in the Supporting Information.

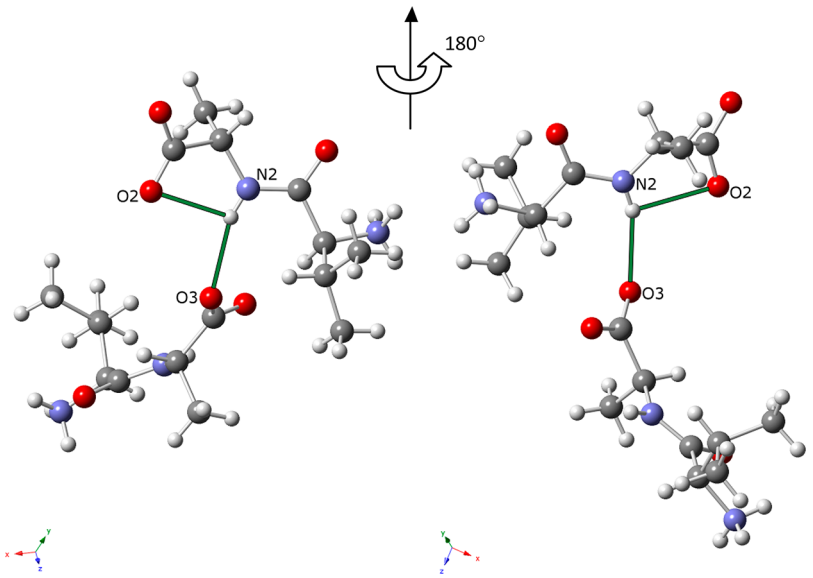

Figure 1. N2 hydrogen-bonding environment from two directions in Val-Ala. The N2 hydrogen may be hydrogen bonded to O2, intramolecularly, or O3, intermolecularly, or both in a three-center bond. Hydrogen bonds are indicated by solid green lines.

convergence are known to be similar for similar systems,[40] convergence testing was not performed for the other peptides. For the disordered structures, calculations were done for each configuration. A weighted average of the resulting shieldings was used.

The calculated shieldings are related to the observed, referenced, chemical shifts according to $\delta_{iso} = \sigma_{ref} - \sigma_{iso}$,[41] where δ_{iso} is the isotropic chemical shift, σ_{iso} is the calculated shielding, and σ_{ref} is chemical shielding value of the reference. Here, σ_{ref} was chosen such that the mean experimental and calculated shift coincided.[41−45] The calculated chemical shift values were then used to assign the resonances to particular carbon resonances. In most cases, assignments were unambiguous. In others, because of very close resonances or calculated shieldings, some assignments are uncertain. The backbone assignments were clear in all cases except the two Cα sites of Ile-Val.

Labeling Scheme. Atom labels are based on the amino acid residue in which they are found, numbering from the N-terminal, and their position within the residue. The α-β-γ notation used here is part of the IUPAC convention for labeling proteins.[46] Hydrogen atoms are discussed using the label of the heavy atom to which they are bonded. For example, the hydrogen bonded to N2 is referred to as the N2 hydrogen. The complete labeling scheme is shown in Figures S1 and S2, and the details of the nomenclature are further discussed.

RESULTS AND DISCUSSION

Crystal Structures. The seven dipeptides form crystal structures with several angstrom diameter 1D pores. Their structures have been discussed in greater detail elsewhere.[26,47,48] All seven dipeptides belong to the $P6_1$ space group, and they exhibit very similar unit cell parameters ($a \sim 14.5$ Å, $b \sim 14.5$ Å, and $c \sim 10.2$ Å), which are given in Table S2. Here, we focus on aspects of the structures relevant to understanding their chemical shifts.

The backbone and side-chain torsion angles of the dipeptides, as determined from their room-temperature crystal structures, are shown in Table 1. Because Ala-Val is slightly disordered over some of the backbone positions, a weighted average is shown in the table; the values for each configuration can be found in the Supporting Information. As expected, the ω torsion angle shows that the amide bond is very nearly planar in all of the dipeptides. The ψ_1 and φ_2 angles are consistent with protein β-sheet secondary structure.

For two of the dipeptides, Ala-Val and Val-Ile, the crystal structure shows disorder that is primarily in the position of the valine side-chain atoms. To distinguish between these positions, they are referred to as configurations A, B, and C for Ala-Val and configurations A and B for Val-Ile. The letters are assigned in the order of decreasing occupancy. Where appropriate, weighted averages of the structural parameters and calculated NMR shifts are used for these structures. Because the minor

dx.doi.org/10.1021/jp411220y | J. Phys. Chem. A 2014, 118, 2618−2628

Table 2. Hydrogen-Bond Donor−Acceptor Distances for Intermolecular Hydrogen Bonds[a]

	Ala-Val	Val-Ala	Ala-Ile	Ile-Ala	Val-Ile	Ile-Val	Val-Val
R_{DA}, N2−O2 (Å)	2.75	2.72	2.75	2.73	2.75	2.77	2.74
R_{DA}, N1−O1 (Å)	2.71	2.73	2.68	2.72	2.84	2.82	2.81
R_{DA}, N1−O2 (Å)	2.73	2.77	2.73	2.78	2.85	2.84	2.82
R_{DA}, N1−O3 (Å)	2.70	2.72	2.73	2.71	2.74	2.75	2.72

[a]Assuming a three-center hydrogen bond. Because Ala-Val is disordered over the carboxyl oxygen atoms, a weighted average is given here. The distances for each configuration and the intramolecular distances can be found in the Supporting Information.

Table 3. Isotropic Chemical Shifts of the Backbone Carbon and Nitrogen Atoms of the Dipeptides[a]

	Ala-Val	Val-Ala	Ala-Ile	Ile-Ala	Val-Ile	Ile-Val	Val-Val
C1	173.7	173.8	174.6	174.3	173.2	173.1	173.5
C2	176.7	178.0	176.9	177.8	176.4	176.7	176.6
Cα1	50.5	60.2	50.5	60.5	61.9	63.9[b]	61.3
Cα2	65.2	54.6	66.0	54.8	63.9	62.8[b]	63.4
N1	−339.1	−350.3	−337.5	−349.3	−348.0	−347.8	−348.8
N2	−252.3	−253.0	−250.8	−252.4	−257.7	−259.3	−259.5

[a]All values are in ppm. [b]Uncertain assignment.

Table 4. Chemical Shift Tensors of the Carbonyl, C1, and Carboxyl, C2, Carbon Atoms and the Amide Nitrogen, N2[a]

		Ala-Val	Val-Ala	Ala-Ile	Ile-Ala	Val-Ile	Ile-Val	Val-Val
C1	δ_{11}	241.04 ± 0.14	240.1 ± 0.2	243.2 ± 0.2	240.1 ± 0.4	242.3 ± 0.2	242.7 ± 0.4	242.2 ± 0.2
	δ_{22}	186.4 ± 0.4	188.2 ± 0.4	187.8 ± 0.6	190.3 ± 0.4	185.1 ± 0.2	184.5 ± 0.1	185.4 ± 0.2
	δ_{33}	93.6 ± 0.5	93.0 ± 0.2	92.8 ± 0.5	92.5 ± 0.2	92.3 ± 0.4	92.2 ± 0.5	92.8 ± 0.4
C2	δ_{11}	238.5 ± 0.3	240.0 ± 0.2	240.2 ± 0.4	241.6 ± 0.4	241.3 ± 0.2	240.8 ± 0.3	239.5 ± 0.3
	δ_{22}	177.6 ± 0.2	179.2 ± 0.2	178.1 ± 0.3	178.3 ± 0.2	176.6 ± 0.3	177.9 ± 0.3	178.1 ± 0.3
	δ_{33}	114.0 ± 0.1	114.7 ± 0.1	112.5 ± 0.1	113.5 ± 0.2	111.3 ± 0.2	111.5 ± 0.2	112.3 ± 0.2
N2	δ_{11}	−147.1	−147.4	−152.1	−144.7	−144.7	−144.9	−150.6
	δ_{22}	−303.6	−305.5	−300.1	−305.9	−312.1	−315.4	−314.0
	δ_{33}	−306.6	−306.0	−300.1	−306.8	−316.2	−317.8	−314.0

[a]All values are in ppm. The uncertainties in carbon shift values are SEM. For N2, the standard deviation is estimated to be ±0.7 in δ_{11}, ±0.15 in δ_{22}, and ±0.7 in δ_{33}.

configurations are more heavily populated for Ala-Val, a new Ala-Val structure was determined. In the published structure,[27] only the side-chain atoms are modeled as occupying multiple positions; in the newly determined structure, several of the valine backbone atoms are instead modeled as occupying multiple closely spaced positions corresponding to particular side-chain configurations. Although these treatments give qualitatively similar structures, the latter is more appropriate for computational work because any fluctuations in these positions resulting from side-chain motion or thermal fluctuations are neglected by CASTEP.

Hydrogen bonding is expected to have a significant influence on the chemical shift. The donor−acceptor distance, R_{DA}, is used as an indicator of the hydrogen-bond strength because the X-ray structures do not provide accurate proton positions. There is some evidence to suggest that the donor−acceptor distance has a stronger influence on chemical shift than the bond angle.[16]

The hydrogen-bonding patterns for the seven dipeptides are qualitatively the same. Briefly, we have two hydrogen-bond donors, the N1 and N2 nitrogen atoms. The N2 amide nitrogen is near two oxygen atoms, O2 and an intramolecular O3. The N2 hydrogen may be hydrogen bonded to only one of these or in a three-center bond with both (Figure 1). The N1 nitrogen is in a pocket formed by four oxygen atoms: O1, O2, and O3 on three adjacent molecules and the intramolecular O1. It is most likely that all four are involved in the hydrogen bonding around N1 through one or more three-center hydrogen bonds. (see the Supporting Information for additional discussion as well as Figures S2−S4.) Görbitz has also proposed that the Cα1 hydrogen may be involved in a weak hydrogen bond with the carboxylate oxygen atoms,[26] although it is unclear if this interaction is significant. Here, we do not consider this type of hydrogen bonding. The hydrogen-bond donor−acceptor distances are shown in Table 2. We have chosen to ignore the intramolecular hydrogen bonds because little variation is seen in their donor−acceptor distances and thus they are unlikely to be useful in explaining differences in the chemical shifts.

Assignments. Resonance assignments, shown for backbone sites in Table 3, were made using NMR-CASTEP. With the exception of Ile-Val, all backbone atom resonance assignments were unambiguous from the calculations and experimental spectra. For Ile-Val, the calculated Cα shifts were essentially identical and could not be used to assign the Cα1 and Cα2 resonances separately. The complete set of calculated and experimental shifts can be found in the Supporting Information. Note that despite the disorder in the Ala-Val and Val-Ile structures only a single resonance is observed for each chemical site, indicating rapid interconversion between configurations. The principal values of the shift tensors for C1, C2, and N2 are given in Table 4.

Cα2 Shifts. On the basis of an accumulation of chemical shift data of proteins, detailed and reliable correlations have

dx.doi.org/10.1021/jp411220y | J. Phys. Chem. A 2014, 118, 2618−2628

been established between Cα chemical shifts and local secondary structure (α-helix, β-sheet, etc.) in the solution phase. The importance of side-chain identity can be seen from the characteristic shifts for valine and isoleucine, which have been given as 9−10 and 9 ppm, respectively, downfield from alanine Cα.[8,49] Although changes in the environment from a liquid to a solid state can lead to significant changes in shift, it is clear from the solution-state data that the chemical identity is an important factor. Although the solution-state chemical shifts point to the importance of residue identity, the interpretation is confounded by the potential for systematic differences in conformation and secondary structure between amino acids. A comparable sequence effect is apparent in our data (Table 3); the minor structural difference between valine and isoleucine does not seem to play an important role.

To investigate further the differences between the valine and isoleucine Cα shifts, we start by considering their dependence on the backbone torsion angles, ϕ_2 and ψ_T. For these dipeptides, Cα2 chemical shifts clearly show a trend toward downfield as ϕ_2 increases, ψ_T decreases (Figure 2), and with χ_{21}

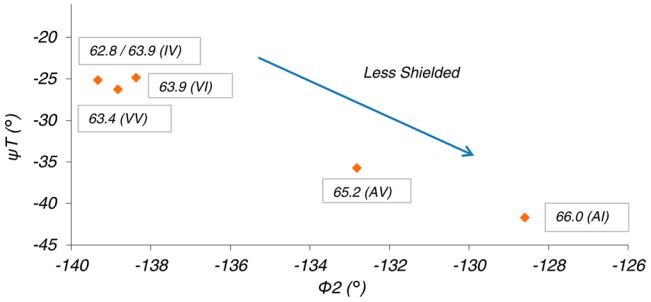

Figure 2. Cα2 chemical shifts show decreased shielding as the backbone torsion angles φ_2 and ψ_T increase and decrease, respectively. Each point is labeled using the two-letter amino acid code (A, Ala; V, Val; and I, Ile) and the Cα2 chemical shift. Two values are given for Ile-Val because of the uncertain Cα assignment.

shifting from ∼60 to ∼ −60°. Given the correlations between the different torsion angles around Cα2 in these samples, from this set of compounds we cannot fully isolate the effects of these factors. In the case of capped leucine, Havlin and co-workers found, through computational studies, that the Cα shift tensor is much more sensitive to the backbone torsion angles than the side-chain angles.[20] Others have found the same result for the backbone angles and only a small shift change because of hydrogen bonding.[50] They have also shown that valine and isoleucine Cα shift tensors behave similarly.[5] Experimentally, Wittebort and co-workers also found the Cα shift in glycyl tripeptides to be strongly dependent on the backbone angles.[51] This is consistent with our findings for leucine and isoleucine in which changes on the order of 10° in ϕ_2 and ψ_T results in a several ppm change in the Cα2 isotropic shift, affirming that the backbone geometry is its primary influence. The Cα2 shift for the valine and isoleucine residues is also correlated to the chemical shift of the adjacent N2 nucleus (Figure 3), which may be explained by through-bond effects or by a shared dependence on secondary structure (see the N2 section in the Results and Discussion).

Previous work by Beger and Bolton predicted that, for amino acid residues including valine and isoleucine, increasing ϕ and decreasing ψ in the region of conformation space inhabited by our dipeptides should result in higher shifts, as we observed for

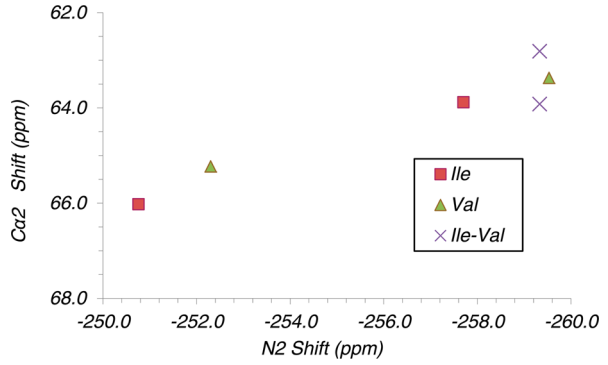

Figure 3. Cα2 shift and N2 shift are strongly correlated. The second residue amino acid corresponding to each point is shown in the legend; Ile-Val shifts for both Cα carbons are shown because the assignment is uncertain.

Cα2 (Figure 2).[49] Although their results are for internal residues, our results suggest they may be more widely applicable. de Dios and co-workers have calculated that, given particular backbone angles (φ = −139°, ψ = 140°), changes in the first χ backbone angle for capped valine in vacuum can lead to changes in Cα of several ppm.[52] In particular, the difference between χ_1 = −60° and χ_1 = 60° was about 0.4 ppm, with the former being more shielded. Assuming similar results at other backbone angles, this work suggests that the differences in backbone angles cannot explain the lower Cα2 shielding of Ala-Val and Ala-Ile.

Cα1 Shifts. Because Cα1 is adjacent to a terminal $^+NH_3$ group, we need to consider only two torsion angles around Cα1, namely, ψ_1 and χ_{11}. If we consider all of the residues, we see in Figure 4 that the Cα1 nucleus becomes deshielded as the

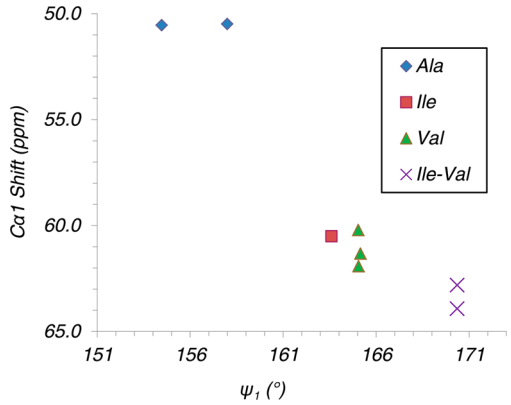

Figure 4. Cα1 chemical shift increases as ψ_1 increases. The first residue amino acid is indicated in the legend. Because of the uncertainty in the assignment, both Cα shifts are included for Ile-Val.

ψ_1 torsion angle increases; we observe no such correlation between the χ_{11} angle and the Cα1 shift (not shown). Through-bond effects may also be responsible for some of the variation; as can be seen in Figure 5, Cα1 becomes deshielded with N1. This is consistent with the trend observed for the isotropic Cα2 and N2 chemical shifts.

C1 Shifts. We expect the C1 chemical shift to be most strongly dependent on the hydrogen-bond strength. The C1 isotropic chemical shift is plotted against the intermolecular donor−acceptor hydrogen-bond distance, R_{DA}, in Figure 6. The data show a compelling overall correlation between the C1 shift

dx.doi.org/10.1021/jp411220y | J. Phys. Chem. A 2014, 118, 2618−2628

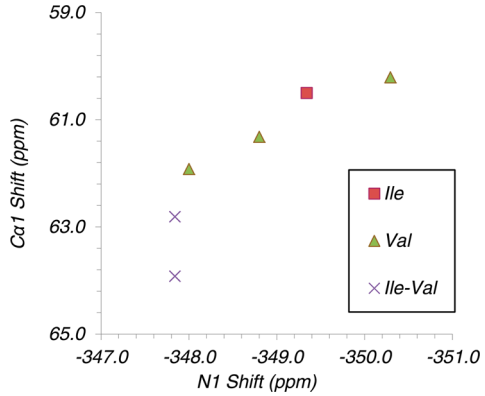

Figure 5. Cα1 and N1 shifts become deshielded together across the peptide series for the Ile and Val residues. The first residue amino acid is indicated in the legend. Because of the uncertainty in the assignment, both Cα shifts are included for Ile-Val.

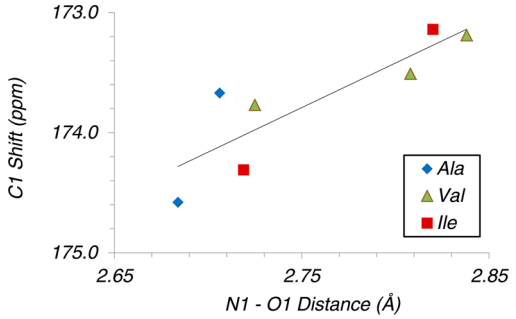

Figure 6. C1 carbonyl carbon chemical shift decreases with increasing hydrogen-bonding distance (r^2 = 0.74). The first residue amino acid is indicated in the legend.

and the intermolecular hydrogen-bonding distance; we discern no clear relationship between the C1 isotropic shifts and amino acid identity, backbone torsion angles, or intramolecular hydrogen-bond distance. It is most likely that the additional observed variation is due to differences in the hydrogen-bond angle, as it is also a contributing factor in the hydrogen-bond strength.[14,15,53] Previous work by Ando and co-workers on carbonyl carbons in glycine residues has shown that increasing the donor−acceptor distance to terminal NH_3^+ groups deshields the carbon,[16] whereas other work shows increasing the distance to internal NH groups increases the shielding.[15,16,54,55] Similarly, computational work on peptide fragments showed that lengthening hydrogen bonds to uncharged NH_2 groups resulted in increased shielding.[56] In our work, we see increased shielding with distance to the NH_3^+ group, suggesting Ando's earlier result with charged hydrogen-bond donor groups may not be generally applicable.

The lack of dependence on the residue identity is noteworthy. In the solution state, characteristic internal carbonyl shifts in β-sheets have been given as 175.1, 174.1, and 174.1 ppm for Ala, Ile, and Val, respectively,[49] and as 176.1, 174.9, and 174.8 ppm for α-helices.[8] Although the solution-state work suggests that the side-chain length might explain some of the variation, we see no evidence for such an effect in our dipeptide data set. This disagreement highlights the difficulty inherent to applying solution-state results to the solid state beyond concerns about packing effects. In general, discrepancies with the solution state reflect different likelihoods of particular conformations or hydrogen-bonding environments in addition to intrinsic differences in the environments around these nuclei.

We also compare the slope of the linear fit for the intermolecular hydrogen bonding, −7.4 ± 2.0 ppm $Å^{-1}$, to values reported in the literature for carbonyl−amide type hydrogen bonds. Slopes have been reported as −18.3 and −21.7 ppm $Å^{-1}$ for alanine residues[15,54] and −14.2 ppm $Å^{-1}$ for valine residues.[55] The slope determined from our data set is an aggregate of three different amino acids; thus, we do not expect the agreement to be exact with the single-residue results reported earlier. Computational work suggests that our dipeptides should have a slope of greater magnitude than these previous results because of nonlinearity in the relationship.[15] This discrepancy suggests that the nature of the hydrogen-bonding partner may have an impact on the observed trend. That is, it appears that the charged hydrogen-bonding donor reduces the sensitivity of the shift to hydrogen-bonding distance.

In interpreting the carbonyl shift tensor principal values, it is helpful to recall the orientation of the tensor principal axis system in the molecular frame. Although the exact orientations vary, previous work has found that δ_{22} is nearly collinear with the C═O bond, with δ_{11} between the C═O bond and the C−N bond and δ_{33} orthogonal to the peptide plane.[17] Because δ_{22} is most closely aligned with the hydrogen bond, it is expected to be the most sensitive to the hydrogen-bonding environment. Computational and experimental work on glycine and alanine residue carbonyl groups has shown relationships between tensor values and hydrogen-bond length to NH and NH_3^+. In both cases, longer hydrogen bonds lead to a decrease in shielding for δ_{11}, an increase for δ_{22}, and little change for δ_{33}.[15,16]

The three principal values of the shielding tensor for C1 in our set of dipeptides are plotted against the donor−acceptor distance in Figure 7. We see trends largely consistent with the above predictions. Most of the δ_{11} values show a downfield shift as the bond distance increases. For δ_{22}, the shifts move upfield with the hydrogen-bond distance. Little variation is seen in δ_{33}. These results are consistent with previous computational work.[56] Because only some of the change in δ_{11} and δ_{22} can be explained using the hydrogen-bond distance, there are likely other important factors including the hydrogen-bond angle and packing effects. It is worth noting that the three upfield δ_{11} values do not share an obvious residue identity connection. Because the chemical shift depends on all of these contributing factors, it is difficult to tease apart individual contributions.

Previous researchers have used a series of compounds with alanine residues to linearly fit the relationship for δ_{22}, with a slope of −63.8 ppm $Å^{-1}$.[54] Another group found a much smaller slope in the same relationship, −30.2 ppm $Å^{-1}$.[57] Limited data for valine residues appeared to be consistent with the fit for alanine in that work. Only a slight, and nearly opposite, dependence on the donor−acceptor distance for the other two components was observed, and the variations between compounds of those values were much smaller (~10 ppm) than the variations in δ_{22} (~30 ppm).[57] A weighted linear fit of the δ_{22} reported here against the N1−O1 hydrogen-bond distance gave a slope of −30 ± 8 ppm $Å^{-1}$, consistent with the results of the second study despite the different hydrogen-bond donor type. We also see much greater variation in δ_{22}, 6 ppm, than in δ_{11}, 3 ppm, or δ_{33}, 1.4 ppm, suggesting that the hydrogen bonding is mostly responsible for the variation.

dx.doi.org/10.1021/jp411220y | J. Phys. Chem. A 2014, 118, 2618−2628

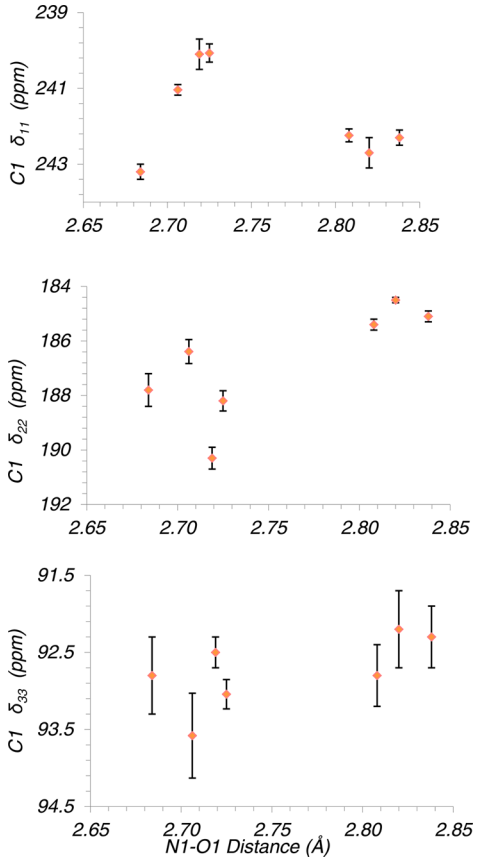

Figure 7. Dependence of the principal values δ_{11}, δ_{22}, and δ_{33} of the C1 chemical shift tensor on the intermolecular N1−O1 hydrogen-bond distance. Error bars are SEM.

C2 Shifts. Given the number of hydrogen-bonding interactions around the C2 carboxyl carbon, interpreting the connection between the shifts and distances and the effect of the carboxyl group's negative charge is more difficult.[58] In Figure 8, the C2 isotropic chemical shift is plotted against the

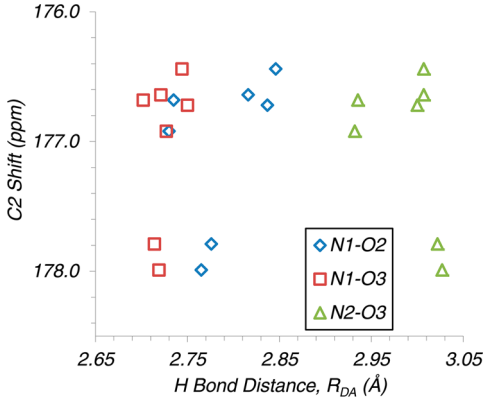

Figure 8. C2 carboxyl carbon chemical shift and the donor−acceptor distances of the potential hydrogen-bonding partners.

three intermolecular hydrogen-bond donor−acceptor distances. The two compounds with significantly deshielded C2 carbons relative to the other dipeptides are Val-Ala and Ile-Ala. Although previous work has suggested that amino acid identity has much less impact, if any, on carboxyl shifts,[14] the large gap between values for these two dipeptides strongly suggests that it may be an important factor. Leaving aside these two compounds, the remaining five show a slight increase in shielding as the hydrogen bonds lengthen.

Characteristic orientations for carboxylate carbon shift tensors are known. As with carbonyl carbons, δ_{33} is perpendicular to the peptide plane. Because of local symmetry, δ_{11} approximately bisects the O−C−O angle.[59] In Figure 9, we consider only the N1−O2 and N2−O3 distances because little variation is seen in the N1−O3 distance.

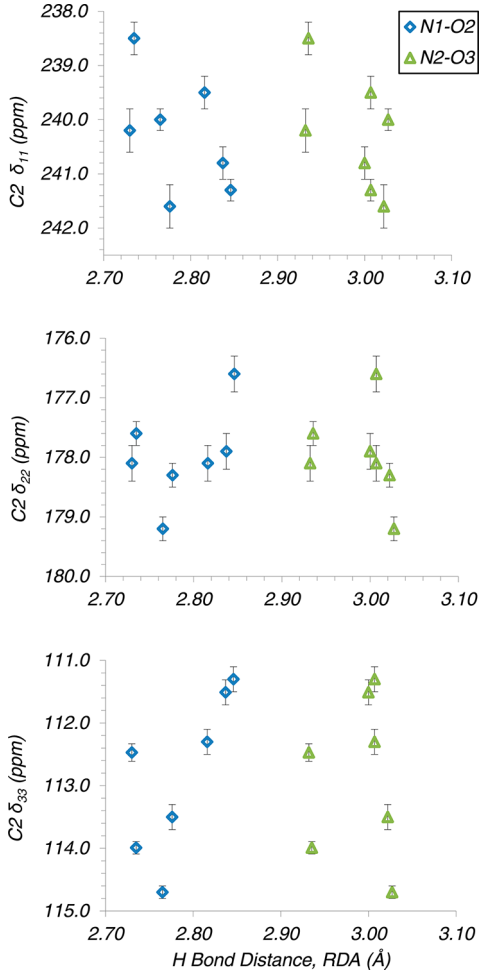

Figure 9. Dependence of the principal values δ_{11}, δ_{22}, and δ_{33} of the C2 chemical shift tensor on the N1−O2 (blue) and N2−O3 (green) hydrogen-bond distances. Error bars are SEM.

The range of each principal value is about the same, approximately 3 to 4 ppm, unlike in the C1 case. None of the principal values is sensitive to hydrogen bonding, perhaps because none of the principal axes lay along a CO bond. The absence of clear trends may reflect more generally on the complexity of the electronic environment around C2 because of the many hydrogen-bonding interactions as well as the anionic nature of the carboxylate group. Others have found that for deprotonated carboxylate carbons in amino acids, stronger hydrogen bonding has been found to result in a decrease in the δ_{22} shift.[14] Although we do not see evidence in support of that finding here, given the complexity of the hydrogen bonding around C2, this result should not be considered as evidence against such a relationship.

dx.doi.org/10.1021/jp411220y | J. Phys. Chem. A 2014, 118, 2618−2628

N2 Amide Shifts. Amide ^{15}N chemical shifts are sensitive to the hydrogen-bonding environment, residue identity, and conformation.[3,60,61] Figure 10 shows the relationship between

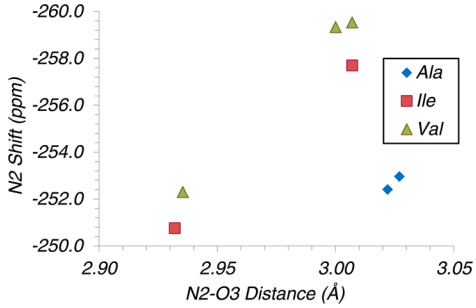

Figure 10. N2 isotropic chemical shifts show dependence on both N2−O3 hydrogen-bonding distance and the residue identity. The inset legend indicates the second amino acid residue.

the intermolecular hydrogen-bond distance and the N2 isotropic chemical shift in our data. Given that previous computational work shows a 10 ppm residue identity effect is reasonable,[18] the isotropic shift data can be most easily explained using the hydrogen-bonding distance, with shielding increasing with the hydrogen-bond distance, consistent with previous computational work by de Dios and co-workers showing that hydrogen bonding resulted in deshielding.[50] Although de Dios et al. also showed a significant ^{15}N dependence on the side-chain angle for valine residues, here only a small range of χ_{21} values are observed.[50] This underscores the utility of using an isostructural series for this study, as the consistency in these values allows us to isolate other factors. Alternatively, the shifts can be explained using the peptide plane angle, ω, and the hydrogen-bond length (see the Supporting Information.)

The N2 tensor data are shown in Figure 11 as a function of the N2 hydrogen-bond length. Previous work has shown that the least shielded component, δ_{11}, points approximately along the hydrogen bond, δ_{22} perpendicular to the peptide plane, and δ_{33} along the N−Cα bond.[62,63] Although δ_{11} shows little dependence on the hydrogen-bond length, δ_{22} and δ_{33} both show a decrease in shielding as the hydrogen bond shortens,[64−66] which is consistent with changes expected from the Ramsey equation. These results are in partial agreement with previous study of the shift tensor of nucleic acid bases, which found that δ_{22} was deshielded by hydrogen bonding, whereas δ_{11} and δ_{33} were shielded.[65] The results are also consistent with the findings of Bhate et al. for alanine and glycine containing dipeptides.[13] The N2 chemical shift tensor components δ_{22} and δ_{33} here also show some correlation with the peptide plane angle ω (see the Supporting Information).

N1 Amine Shifts. As with the C2 carboxylate carbon shift, multiple hydrogen-bond distances affect the N1 amine nitrogen shift. The three relevant intermolecular donor−acceptor distances are the N1−O1, N1−O2, and N1−O3 distances. Additionally, there may be an intramolecular hydrogen bond between N1 and O1. The dipeptides where alanine is the first residue, Ala-Val and Ala-Ile, have N1 shifts that are 10 ppm deshielded, consistent with the first N2 isotropic shift explanation. The importance of the intermolecular hydrogen-bond donor−acceptor distances for the other five dipeptides can be seen in Figure 12. Because these distances are closely related to each other, we cannot determine the relative

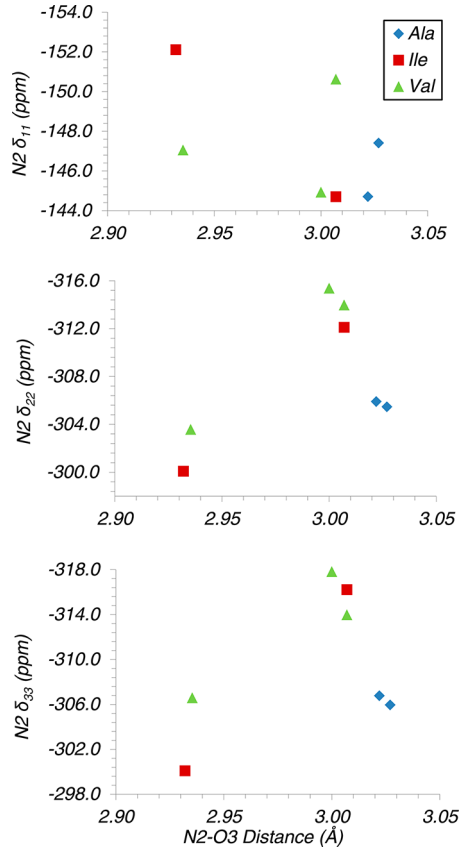

Figure 11. Chemical shift tensor principal components δ_{11}, δ_{22}, and δ_{33} for the N2 nitrogen. The legend indicates the second residue amino acid. The standard deviation is estimated to be ±0.7 in δ_{11}, ±0.15 in δ_{22}, and ±0.7 in δ_{33} for each of the principal components of N2 reported.

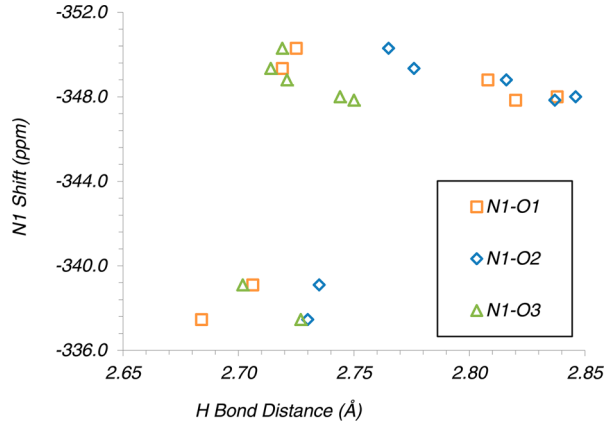

Figure 12. N1 chemical shift dependence on the three intermolecular hydrogen-bond donor−acceptor distances for N1. The two relatively deshielded N1 shifts are from Ala-Val and Ala-Ile.

importance of the various donor−acceptor distances. However, the overall trend is clear: as the hydrogen bonds shorten, shielding increases. Note that the full shift tensors for N1 were not determined because terminal NH_3^+ groups have little anisotropy as a result of their nearly symmetric environment.

CONCLUSIONS

We have presented here trends in solid-state chemical shifts dependent on chemical identity, conformation, and hydrogen

dx.doi.org/10.1021/jp411220y | J. Phys. Chem. A 2014, 118, 2618−2628

bonding for a series of seven isostructural dipeptides. Foreknowledge of the crystal structures allows us to correlate the chemical shift data to structural parameters and thus to put the interpretation of NMR data on a more rigorous footing. Although no single set of compounds can definitively link structure and chemical shift, the results obtained for several of the backbone atomic sites in our data set are encouraging and add to a growing library of experimental data in this area. Indeed, crystalline dipeptides have contributed valuable chemical shift tensor information to this library.[67−69] Our data shows that three essential factors influence the Cα chemical shifts: residue position, amino acid identity, and the local conformation around the Cα site. This bears similarity to what is seen in chemical shifts in proteins in the solution state for Cα carbons. The internal C1 carbonyl carbon isotropic shifts, along with its δ_{22} component, are strongly dependent on the hydrogen-bond donor−acceptor distance, whereas the δ_{33} component is nearly invariant to this distance. Our results suggest that the C2 carboxyl carbon chemical shift depends on both the amino acid identity and the hydrogen bonding. The C2 shift tensor principal values show variances similar to those of C1 principal values, although we do not discern any clear relationships between the C2 principal values and hydrogen bonding. This may be a consequence of the complexity of the hydrogen-bonding network. The amide N2 shifts appear to be strongly influenced by the hydrogen-bonding environment, with δ_{22} and δ_{33} about equally affected. Despite our focus on compounds with very similar structures, our analysis yielded a mix of strong and weak structure−shift correlations, which we attribute to the extreme sensitivity of chemical shift to local structure and hydrogen bonding.

Our results point to further work with these dipeptides that will shed additional light on the trends reported here. This type of analysis would certainly benefit from additional compounds. Although all seven known dipeptides in this isostructural series are included in our study, it may be possible to prepare others using artificial amino acids similar to valine and isoleucine. Cocrystallizing two or more dipeptides into a single crystal structure could allow for the study of additional geometries. Lastly, conducting similar studies on other sets of isostructural compounds, such as the Leu-Leu family of porous dipeptides,[70] would help to confirm that the trends reported here apply more generally.

■ ASSOCIATED CONTENT

Supporting Information

Site labeling scheme, unit cell parameters, structural data, discussion of hydrogen bonding, dependence of N2 chemical shift principal components on ω, calculated and experimental shifts, solid-state NMR and PXRD data, and Herzfeld−Berger analyses of spinning side bands. This material is available free of charge via the Internet at http://pubs.acs.org.

■ AUTHOR INFORMATION

Corresponding Author

*E-mail: manish.mehta@oberlin.edu.

Notes

The authors declare no competing financial interest.

■ ACKNOWLEDGMENTS

This work was supported by NSF RUI grant CHE-1012813, NSF-MRI grant DMR-0922588 for the acquisition of a powder X-ray diffractometer, and a Henry Dreyfus Teacher-Scholar grant (M.A.M.) from the Camille and Henry Dreyfus Foundation. The single-crystal X-ray diffractometer at Youngstown State University (YSU) was funded by NSF grant 0087210, Ohio Board of Regents grant CAP-491, and YSU. We gratefully acknowledge assistance from Dr. Matthias Zeller at YSU for the solution of the Ala-Val structure.

■ REFERENCES

(1) Cavalli, A.; Salvatella, X.; Dobson, C. M.; Vendruscolo, M. Protein Structure Determination from NMR Chemical Shifts. *Proc. Natl. Acad. Sci. U.S.A.* **2007**, *104*, 9615−9620.

(2) Shen, Y.; Lange, O.; Delaglio, F.; Rossi, P.; Aramini, J. M.; Liu, G.; Eletsky, A.; Wu, Y.; Singarapu, K. K.; Lemak, A.; et al. Consistent Blind Protein Structure Generation from NMR Chemical Shift Data. *Proc. Natl. Acad. Sci. U.S.A.* **2008**, *105*, 4685−4690.

(3) Saitô, H.; Ando, I.; Ramamoorthy, A. Chemical Shift Tensor − The Heart of NMR: Insights into Biological Aspects of Proteins. *Prog. Nucl. Magn. Reson. Spectrosc.* **2010**, *57*, 181−228.

(4) Vila, J. A.; Aramini, J. M.; Rossi, P.; Kuzin, A.; Su, M.; Seetharaman, J.; Xiao, R.; Tong, L.; Montelione, G. T.; Scheraga, H. A. Quantum Chemical ^{13}C(Alpha) Chemical Shift Calculations for Protein NMR Structure Determination, Refinement, and Validation. *Proc. Natl. Acad. Sci. U.S.A.* **2008**, *105*, 14389−14394.

(5) Havlin, R. H.; Le, H.; Laws, D. D.; de Dios, A. C.; Oldfield, E. An Ab Initio Quantum Chemical Investigation of Carbon-13 NMR Shielding Tensors in Glycine, Alanine, Valine, Isoleucine, Serine, and Threonine: Comparisons between Helical and Sheet Tensors, and the Effects of χ1 on Shielding. *J. Am. Chem. Soc.* **1997**, *119*, 11951−11958.

(6) Heller, J.; Laws, D. D.; Tomaselli, M.; King, D. S.; Wemmer, D. E.; Pines, A.; Havlin, R. H.; Oldfield, E. Determination of Dihedral Angles in Peptides through Experimental and Theoretical Studies of α-Carbon Chemical Shielding Tensors. *J. Am. Chem. Soc.* **1997**, *119*, 7827−7831.

(7) Wylie, B. J.; Schwieters, C. D.; Oldfield, E.; Rienstra, C. M. Protein Structure Refinement Using ^{13}Cα Chemical Shift Tensors. *J. Am. Chem. Soc.* **2009**, *131*, 985−992.

(8) Zhang, H.; Neal, S.; Wishart, D. S. RefDB: A Database of Uniformly Referenced Protein Chemical Shifts. *J. Biomol. NMR* **2003**, *25*, 173−195.

(9) Wang, Y.; Jardetzky, O. Investigation of the Neighboring Residue Effects on Protein Chemical Shifts. *J. Am. Chem. Soc.* **2002**, *124*, 14075−14084.

(10) Hong, M. Solid-State NMR Determination of ^{13}Cα Chemical Shift Anisotropies for the Identification of Protein Secondary Structure. *J. Am. Chem. Soc.* **2000**, *122*, 3762−3770.

(11) Lee, D. K.; Wittebort, R. J.; Ramamoorthy, A. Characterization of ^{15}N Chemical Shift and ^{1}H−^{15}N Dipolar Coupling Interactions in a Peptide Bond of Uniaxially Oriented and Polycrystalline Samples by One-Dimensional Dipolar Chemical Shift Solid-State NMR Spectroscopy. *J. Am. Chem. Soc.* **1998**, *120*, 8868−8874.

(12) Tjandra, N.; Bax, A. Large Variations in ^{13}Cα Chemical Shift Anisotropy in Proteins Correlate with Secondary Structure. *J. Am. Chem. Soc.* **1997**, *119*, 9576−9577.

(13) Bhate, M. P.; Woodard, J. C.; Mehta, M. A. Solvation and Hydrogen Bonding in Alanine- and Glycine-Containing Dipeptides Probed Using Solution- and Solid-State NMR Spectroscopy. *J. Am. Chem. Soc.* **2009**, *131*, 9579−9589.

(14) Gu, Z.; Zambrano, R.; McDermott, A. Hydrogen Bonding of Carboxyl Groups in Solid-State Amino Acids and Peptides: Comparison of Carbon Chemical Shielding, Infrared Frequencies, and Structures. *J. Am. Chem. Soc.* **1994**, *116*, 6368−6372.

(15) Asakawa, N.; Kuroki, S.; Kurosu, H.; Ando, I.; Shoji, A.; Ozaki, T. Hydrogen-Bonding Effect on Carbon-13 NMR Chemical Shifts of L-Alanine Residue Carbonyl Carbons of Peptides in the Solid State. *J. Am. Chem. Soc.* **1992**, *114*, 3261−3265.

(16) Ando, S.; Ando, I.; Shoji, A.; Ozaki, T. Intermolecular Hydrogen-Bonding Effect on Carbon-13 NMR Chemical Shifts of

Glycine Residue Carbonyl Carbons of Peptides in the Solid State. *J. Am. Chem. Soc.* **1988**, *110*, 3380−3386.
(17) Oas, T. G.; Hartzell, C. J.; McMahon, T. J.; Drobny, G. P.; Dahlquist, F. W. The Carbonyl Carbon-13 Chemical Shift Tensors of Five Peptides Determined from Nitrogen-15 Dipole-Coupled Chemical Shift Powder Patterns. *J. Am. Chem. Soc.* **1987**, *109*, 5956−5962.
(18) Poon, A.; Birn, J.; Ramamoorthy, A. How Does an Amide-^{15}N Chemical Shift Tensor Vary in Peptides? *J. Phys. Chem. B* **2004**, *108*, 16577−16585.
(19) Birn, J.; Poon, A.; Mao, Y.; Ramamoorthy, A. Ab Initio Study of $^{13}C_{\alpha}$ Chemical Shift Anisotropy Tensors in Peptides. *J. Am. Chem. Soc.* **2004**, *126*, 8529−8534.
(20) Havlin, R. H.; Laws, D. D.; Bitter, H. M.; Sanders, L. K.; Sun, H.; Grimley, J. S.; Wemmer, D. E.; Pines, A.; Oldfield, E. An Experimental and Theoretical Investigation of the Chemical Shielding Tensors of $^{13}C\alpha$ Of Alanine, Valine, and Leucine Residues in Solid Peptides and in Proteins in Solution. *J. Am. Chem. Soc.* **2001**, *123*, 10362−10369.
(21) Harris, R. K. NMR Crystallography: The Use of Chemical Shifts. *Solid State Sci.* **2004**, *6*, 1025−1037.
(22) Goward, G. R.; Sebastiani, D.; Schnell, I.; Spiess, H. W.; Kim, H.-D.; Ishida, H. Benzoxazine Oligomers: Evidence for a Helical Structure from Solid-State NMR Spectroscopy and DFT-Based Dynamics and Chemical Shift Calculations. *J. Am. Chem. Soc.* **2003**, *125*, 5792−5800.
(23) Petkova, A. T.; Ishii, Y.; Balbach, J. J.; Antzutkin, O. N.; Leapman, R. D.; Delaglio, F.; Tycko, R. A Structural Model for Alzheimer's Beta-Amyloid Fibrils Based on Experimental Constraints From Solid State NMR. *Proc. Natl. Acad. Sci. U.S.A.* **2002**, *99*, 16742−16747.
(24) Harris, R. K.; Ghi, P. Y.; Hammond, R. B.; Ma, C.-Y.; Roberts, K. J. Refinement of Hydrogen Atomic Position in a Hydrogen Bond Using a Combination of Solid-State NMR and Computation. *Chem. Commun.* **2003**, 2834−2835.
(25) Olejniczak, S.; Mikuła-Pacholczyk, J.; Hughes, C. E.; Potrzebowski, M. J. ^{15}N and ^{13}C High-Resolution Solid-State NMR Study of the Polymorphism of the L-Enantiomer of N-Benzoylphenylalanine. *J. Phys. Chem. B* **2008**, *112*, 1586−1593.
(26) Görbitz, C. H. Microporous Organic Materials from Hydrophobic Dipeptides. *Chem.—Eur. J.* **2007**, *13*, 1022−1031.
(27) Soldatov, D. V.; Moudrakovski, I. L.; Ripmeester, J. A. Dipeptides as Microporous Materials. *Angew. Chem., Int. Ed.* **2004**, *43*, 6308−6311.
(28) Afonso, R.; Mendes, A.; Gales, L. Peptide-Based Solids: Porosity and Zeolitic Behavior. *J. Mater. Chem.* **2012**, *22*, 1709−1723.
(29) Görbitz, C. H. Nanotubes from Hydrophobic Dipeptides: Pore Size Regulation through Side Chain Substitution. *New J. Chem.* **2003**, *27*, 1789−1793.
(30) Soldatov, D. V.; Moudrakovski, I. L.; Grachev, E. V.; Ripmeester, J. A. Micropores in Crystalline Dipeptides as Seen from the Crystal Structure, He Pycnometry, and ^{129}Xe NMR Spectroscopy. *J. Am. Chem. Soc.* **2006**, *128*, 6737−6744.
(31) Allen, F. H. The Cambridge Structural Database: A Quarter of a Million Crystal Structures and Rising. *Acta Crystallogr., Sect. B* **2002**, *58*, 380−388.
(32) Bräuniger, T.; Wormald, P.; Hodgkinson, P. Improved Proton Decoupling in NMR Spectroscopy of Crystalline Solids Using the SPINAL-64 Sequence. In *Current Developments in Solid State NMR Spectroscopy*; Müller, H.-J., Madhu, P. K., Eds.; Springer: Vienna, Austria, 2003; pp 69−74.
(33) Morcombe, C. R.; Zilm, K. W. Chemical Shift Referencing in MAS Solid State NMR. *J. Magn. Reson.* **2003**, *162*, 479−486.
(34) Hayashi, S.; Hayamizu, K. Chemical Shift Standsrds in High-Resolution Solid-State NMR (2) ^{15}N Nuclei. *Bull. Chem. Soc. Jpn.* **1991**, *64*, 688−690.
(35) Herzfeld, J.; Berger, A. E. Sideband Intensities in NMR Spectra of Samples Spinning at the Magic Angle. *J. Chem. Phys.* **1980**, *73*, 6021−6030.
(36) Eichle, K.; Wasylishen, R. *HBA*; Universität Tübingen: Tübingen, Germany, 2005.
(37) Clark, S. J.; Segall, M. D.; Pickard, C. J.; Hasnip, P. J.; Probert, M. I. J.; Refson, K.; Payne, M. C. First Principles Methods Using CASTEP. Z. Kristallogr. **2005**, *220*.
(38) Yates, J.; Pickard, C.; Mauri, F. Calculation of NMR Chemical Shifts for Extended Systems Using Ultrasoft Pseudopotentials. *Phys. Rev. B* **2007**, *76*, 024401−1−024401−11.
(39) Pickard, C.; Mauri, F. All-Electron Magnetic Response with Pseudopotentials: NMR Chemical Shifts. *Phys. Rev. B* **2001**, *63*, 245101−1−245101−13.
(40) Vasconcelos, F.; Cristol, S.; Paul, J.-F.; Montagne, L.; Mauri, F.; Delevoye, L. First-Principles Calculations of NMR Parameters for Phosphate Materials. *Magn. Reson. Chem.* **2010**, *48*, S142−S150.
(41) Charpentier, T. The PAW/GIPAW Approach for Computing NMR Parameters: A New Dimension Added to NMR Study of Solids. *Solid State Nucl. Magn. Reson.* **2011**, *40*, 1−20.
(42) Webber, A. L.; Elena, B.; Griffin, J. M.; Yates, J. R.; Pham, T. N.; Mauri, F.; Pickard, C. J.; Gil, A. M.; Stein, R.; Lesage, A.; et al. Complete ^{1}H Resonance Assignment of β-Maltose from ^{1}H-^{1}H DQ-SQ Cramps and ^{1}H (DQ-DUMBO)-^{13}C SQ Refocused Inept 2D Solid-State NMR Spectra and First Principles GIPAW Calculations. *Phys. Chem. Chem. Phys.* **2010**, *12*, 6970−6983.
(43) Harris, R. K.; Hodgkinson, P.; Pickard, C. J.; Yates, J. R.; Zorin, V. Chemical Shift Computations on a Crystallographic Basis: Some Reflections and Comments. *Magn. Reson. Chem.* **2007**, *45*, S174−S186.
(44) Gervais, C.; Dupree, R.; Pike, K. J.; Bonhomme, C.; Profeta, M.; Pickard, C. J.; Mauri, F. Combined First-Principles Computational and Experimental Multinuclear Solid-State NMR Investigation of Amino Acids. *J. Phys. Chem. A* **2005**, *109*, 6960−6969.
(45) Gervais, C.; Profeta, M.; Lafond, V.; Bonhomme, C.; Azaïs, T.; Mutin, H.; Pickard, C. J.; Mauri, F.; Babonneau, F. Combined Ab Initio Computational and Experimental Multinuclear Solid-State Magnetic Resonance Study of Phenylphosphonic Acid. *Magn. Reson. Chem.* **2004**, *42*, 445−452.
(46) Markley, J. L.; Bax, A.; Arata, Y.; Hilbers, C. W.; Kaptein, R.; Sykes, B. D.; Wright, P. E.; Wüthrich, K. Recommendations for the Presentation of NMR Structures of Proteins and Nucleic Acids. *J. Mol. Biol.* **1998**, *280*, 933−952.
(47) Görbitz, C. H. An Exceptionally Stable Peptide Nanotube System with Flexible Pores. *Acta Crystallogr., Sect. B* **2002**, *58*, 849−854.
(48) Görbitz, C. H.; Gundersen, E. L-Valyl-L-Alanine. *Acta Crystallogr., Sect. C* **1996**, *52*, 1764−1767.
(49) Beger, R. D.; Bolton, P. H. Protein Phi and Psi Dihedral Restraints Determined from Multidimensional Hypersurface Correlations of Backbone Chemical Shifts and Their Use in the Determination of Protein Tertiary Structures. *J. Biomol. NMR* **1997**, *10*, 129−142.
(50) de Dios, A. C.; Pearson, J. G.; Oldfield, E. Secondary and Tertiary Structural Effects on Protein NMR Chemical Shifts: An Ab Initio Approach. *Science* **1993**, *260*, 1491−1496.
(51) Chekmenev, E. Y.; Xu, R. Z.; Mashuta, M. S.; Wittebort, R. J. Glycyl Cα Chemical Shielding in Tripeptides: Measurement by Solid-State NMR and Correlation with X-ray Structure and Theory. *J. Am. Chem. Soc.* **2002**, *124*, 11894−11899.
(52) de Dios, A. C.; Pearson, J. G.; Oldfield, E. Chemical Shifts in Proteins: An Ab Initio Study of Carbon-13 Nuclear Magnetic Resonance Chemical Shielding in Glycine, Alanine, and Valine Residues. *J. Am. Chem. Soc.* **1993**, *115*, 9768−9773.
(53) Gilli, G.; Gilli, P. *The Nature of the Hydrogen Bond: Outline of a Comprehensive Hydrogen Bond Theory*; Oxford University Press: Oxford, 2009; Vol. 23.
(54) Wei, Y.; Lee, D.-K.; Ramamoorthy, A. Solid-State ^{13}C NMR Chemical Shift Anisotropy Tensors of Polypeptides. *J. Am. Chem. Soc.* **2001**, *123*, 6118−6126.
(55) Tsuchiya, K.; Takahashi, A.; Takeda, N.; Asakawa, N. Hydrogen-Bonding Effect on ^{13}C NMR Chemical Shifts of Amino Acid Residue

Carbonyl Carbons of Some Peptides in the Crystalline State. *J. Mol. Struct.* **1995**, *350*, 233−240.
(56) de Dios, A. C.; Oldfield, E. Chemical Shifts of Carbonyl Carbons in Peptides and Proteins. *J. Am. Chem. Soc.* **1994**, *116*, 11485−11488.
(57) Kameda, T.; Takeda, N.; Kuroki, S.; Kurosu, H.; Ando, S.; Ando, I.; Shoji, A.; Ozaki, T. Hydrogen-Bonded Structure and ^{13}C NMR Chemical Shift Tensor of Amino Acid Residue Carbonyl Carbons of Peptides and Polypeptides in the Crystalline State. Part I. *J. Mol. Struct.* **1996**, *384*, 17−23.
(58) de Dios, A. C.; Laws, D. D.; Oldfield, E. Predicting Carbon-13 Nuclear Magnetic Resonance Chemical Shielding Tensors in Zwitterionic L-Threonine and L-Tyrosine via Quantum Chemistry. *J. Am. Chem. Soc.* **1994**, *116*, 7784−7786.
(59) Gu, Z.; McDermott, A. Chemical Shielding Anisotropy of Protonated and Deprotonated Carboxylates in Amino Acids. *J. Am. Chem. Soc.* **1993**, *115*, 4282−4285.
(60) Chekmenev, E. Y.; Zhang, Q.; Waddell, K. W.; Mashuta, M. S.; Wittebort, R. J. ^{15}N Chemical Shielding in Glycyl Tripeptides: Measurement by Solid-State NMR and Correlation with X-ray Structure. *J. Am. Chem. Soc.* **2004**, *126*, 379−384.
(61) Le, H.; Oldfield, E. Ab Initio Studies of Amide-^{15}N Chemical Shifts in Dipeptides: Applications to Protein NMR Spectroscopy. *J. Phys. Chem.* **1996**, *100*, 16423−16428.
(62) Wylie, B. J.; Sperling, L. J.; Nieuwkoop, A. J.; Franks, W. T.; Oldfield, E.; Rienstra, C. M. Ultrahigh Resolution Protein Structures Using NMR Chemical Shift Tensors. *Proc. Natl. Acad. Sci. U.S.A.* **2011**, *108*, 16974−16979.
(63) Waddell, K. W.; Chekmenev, E. Y.; Wittebort, R. J. Single-Crystal Studies of Peptide Prolyl and Glycyl ^{15}N Shielding Tensors. *J. Am. Chem. Soc.* **2005**, *127*, 9030−9035.
(64) Koder, R. L.; Walsh, J. D.; Pometun, M. S.; Dutton, P. L.; Wittebort, R. J.; Miller, A.-F. ^{15}N Solid-State NMR Provides a Sensitive Probe of Oxidized Flavin Reactive Sites. *J. Am. Chem. Soc.* **2006**, *128*, 15200−15208.
(65) Hu, J. Z.; Facelli, J. C.; Alderman, D. W.; Pugmire, R. J.; Grant, D. M. ^{15}N Chemical Shift Tensors in Nucleic Acid Bases. *J. Am. Chem. Soc.* **1998**, *120*, 9863−9869.
(66) Ramsey, N. F. Magnetic Shielding of Nuclei in Molecules. *Phys. Rev.* **1950**, *78*, 699−703.
(67) Cheng, F.; Sun, H.; Zhang, Y.; Mukkamala, D.; Oldfield, E. A Solid State ^{13}C NMR, Crystallographic, and Quantum Chemical Investigation of Chemical Shifts and Hydrogen Bonding in Histidine Dipeptides. *J. Am. Chem. Soc.* **2005**, *127*, 12544−12554.
(68) Hartzell, C. J.; Pratum, T. K.; Drobny, G. Mutual Orientation of Three Magnetic Tensors in a Polycrystalline Dipeptide by Dipole-Modulated ^{15}N Chemical Shift Spectroscopy. *J. Chem. Phys.* **1987**, *87*, 4324.
(69) Stark, R. E.; Jelinski, L. W.; Ruben, D. J.; Torchia, D. A.; Griffin, R. G. ^{13}C Chemical Shift and $^{13}C-^{15}N$ Dipolar Tensors for the Peptide Bond: [1-^{13}C]Glycyl[^{15}N]Glycine·HCl·H_2O. *J. Magn. Reson.* **1983**, *55*, 266−273.
(70) Görbitz, C. H. Nanotube Formation by Hydrophobic Dipeptides. *Chem.—Eur. J.* **2001**, *7*, 5153−5159.